Facile preparation and characterization of lanthanum-loaded carboxylated multi-walled carbon nanotubes and their application for the adsorption of phosphate ions

Enmin Zong[1], Xiaohuan Liu[2,*], Jifu Wang[3], Shenxiang Yang[2], Jinhua Jiang[1], and Shenyuan Fu[2]

[1] Zhejiang Provincial Key Laboratory of Plant Evolutionary Ecology and Conservation, Taizhou University, Taizhou 318000, People's Republic of China

[2] School of Engineering, and National Engineering and Technology Research Center of Wood-based Resources Comprehensive Utilization, Zhejiang Agriculture and Forestry University, Hangzhou, Lin'an 311300, People's Republic of China

[3] Jiangsu Key Laboratory of Biomass Energy and Material, Institute of Chemical Industry of Forest Products, CAF, Nanjing 210037, People's Republic of China

Received: 8 September 2016
Accepted: 28 February 2017
Published online: 9 March 2017

ABSTRACT

A new carboxylated multi-walled carbon nanotubes adsorbent modified with lanthanum hydroxide (MWCNTs-COOH-La) was prepared, characterized and investigated for phosphate removal in batch experiments. The maximum adsorption capacity of the MWCNTs-COOH-La was 48.02 mg P g^{-1} according to Langmuir model. Structural characterizations demonstrated that the MWCNTs-COOH-La was successfully synthesized and La species was present in the form of $La(OH)_3$. Batch experiments were performed under various conditions (e.g., initial concentrations, temperature, pH, co-existing ions) to investigate the removal of phosphate by MWCNTs-COOH-La. Equilibrium data agreed very well with the Langmuir model, suggesting that the adsorption feature was monolayer. The adsorption behaviors of phosphate were described better by the pseudo-second-order, indicating that the adsorption behaviors were mainly ascribed to chemic-sorption. Phosphate adsorption varied slightly at pH 3–7, but decreased significantly at higher pH values. Phosphate adsorption was slightly influenced by solution ionic strength. A high selectivity of phosphate was also observed in the presence of co-existing anions (except CO_3^{2-}). The underlying mechanism for the specific adsorption of phosphate by MWCNTs-COOH-La was fully analyzed by X-ray diffraction, Fourier transform infrared spectroscopy and X-ray photoelectron spectroscopy technologies. The above results revealed that the hydroxyl groups were involved in the sorption of phosphate and $LaPO_4$ was formed during the adsorption process. This study implied that MWCNTs-COOH-La might be an alternatively viable and promising adsorbent for removal of phosphate from aqueous solution.

Address correspondence to E-mail: liuxiaohuancaf@163.com

Introduction

Phosphorous as an essential nutrient element supports the growth of all organisms in aquatic environment [1]. The presence of different forms of phosphorus in wastewater was organic orthophosphate, phosphate and polyphosphate [2], but only phosphate can be directly assimilated by microorganisms and algae [3]. However, an excessive release of phosphate into fresh waters can speed up the growth of algae and aquatic plants that could release neuro- and hepatotoxins, which negatively affects the environment and public health [4, 5]. On the other side, many countries have established stringent legislations to suppress phosphate discharge. For example, the Environmental Protection Agency (EPA) recommended permissible limit in the stringent discharge to be 0.05 mg L^{-1} for phosphate and the Florida Everglades Forever Act also recommended a mandate of 0.01 mg L^{-1} of phosphate in water [6, 7]. Hence, it is in high demand to develop effective techniques to treat phosphate-rich effluent prior to flowing into aquatic environment [8].

Various strategies for the abatement of phosphate have been developed, such as chemical precipitation [9], crystallization [10], ion exchange [11] and biological treatment [12]. Among these available approaches, adsorption is widely recommended as a most attractive approach with the advantage of its economical and simple operation with low sludge production [13–16]. However, conventional adsorbents did not provide specific interactions with the targeted phosphate ions resulting to low adsorption capacity and selectivity. Consequently, a new efficient and selective absorbent is urgently required to be designed and prepared.

It is well known that the hydrated metal oxides, such as Zr(IV) [17, 18], Fe(III) [19], La(III) [20] and Ce(IV) [21], were extensively explored for abatement of phosphate which could provide lots of coordination sites and possess specific affinity toward phosphate [22]. Among them, lanthanum has attracted widely attention attributed to its innocuous, low-cost, chemically stable and extremely high affinity for phosphate even at low concentrations [23]. Nevertheless, conventional nanostructure commonly showed a strong tendency to aggregate to reduce its surface energy, which reduced the surface available on the nanoparticle and remarkly decreased and the available active species for phosphate removal [3]. As a consequence, a host material is needed which can support an accessible, functional dispersion of lanthanum to improve the dispersion of active species and enhance their adsorption capacities [24].

Carbon nanotubes (CNTs), including multi-wall (MWCNTs) and single-wall (SWCNTs), have been extensively used as a unique host for adsorption materials due to their large specific surface area, layered structures and stability [25, 26]. For instance, alumina supported on multi-walled carbon nanotubes (Al_2O_3/MWCNTs) was an effective adsorbent for simultaneous removal of cadmium ion and trichloroethylene [27]. Manganese oxide-coated carbon nanotubes (MnO_2/CNTs) were demonstrated to be effective for lead removal from aqueous solution [28]. Ceria supported on carbon nanotubes (CeO_2/CNTs) was developed for the removal of arsenate from water [29]. Alumina-coated multi-walled carbon nanotubes composites (Al_2O_3/MWCNTs) exhibited favorable adsorption performance toward lead [25]. These metal oxide-loaded MWCNTs composites possessed larger surface area, better orientation degree and exhibit high adsorption capacities and selectivity for contaminants [25, 27]. Current studies mainly focused on the adsorption of heavy metal and organic contaminants by metal oxide-loaded MWCNTs composites. It is noteworthy that to our knowledge, no study has reported the utilization of lanthanum-modified car-

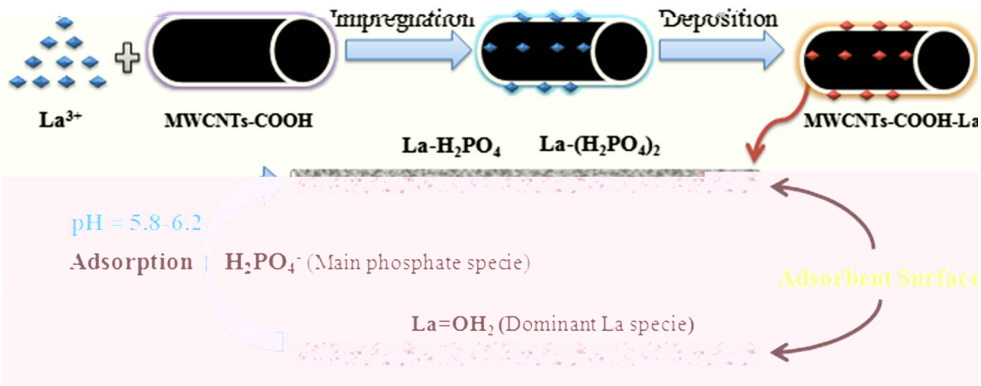

Scheme 1 Schematic presentation of $La(OH)_3$-modified MWCNTs-COOH composite and adsorption process.

Chemicals and methods

Chemicals

Carboxylated multi-walled carbon nanotubes (MWCNTs-COOH) used in the present study were purchased from Chengdu Organic Co., Ltd., Chinese Academy of Sciences. Lanthanum(III) nitrate hydrate was purchased from Sinopharm Chemical Reagent co., Ltd, China. The other chemical reagents such as KH_2PO_4, NaCl, KNO_3, K_2SO_4, $KHCO_3$, K_2CO_3, NaOH, HCl were purchased from Sinopharm Chemical Reagent co., Ltd. All the chemicals were used as obtained without any further purification. Deionized (DI) water was used throughout all the experiments.

Preparation of lanthanum(III)-loaded carboxylic multiple-walled carbon nanotubes (MWCNTs-COOH-La)

Phosphate adsorbent, $La(OH)_3$-loaded MWCNTs-COOH (MWCNTs-COOH-La), was prepared according to previously reported literature method [20, 30] with some modifications. Lanthanum(III) nitrate hydrate was introduced as the lanthanum precursor to incorporate into MWCNTs-COOH, which was expected to form a lanthanum hydroxide composite that would possess highly effective adsorption toward phosphate. In a typical procedure, a suspension containing 4.0 g of MWCNTs-COOH and 200.0 mL deionized water was stirred continuously for 3 h to achieve a uniform MWCNTs-COOH aqueous mixture. Afterward, predetermined amount of lanthanum(III) nitrate hydrate (0.03 M) was slowly added into the above MWCNTs-COOH aqueous mixture. The formed mixture aqueous was stirred at 60 °C for 24 h before raising the solution pH to 10.0 using NaOH solution (0.05 M). The solids were collected, washed with deionized (DI) water until neutral pH. The precipitation was dried in vacuum until a constant weight was reached, and the resulting product was denoted as MWCNTs-COOH-La. The obtained MWCNTs-COOH-La was stored in a desiccator for further phosphate adsorption studies. The detailed synthetic strategy for the MWCNTs-COOH-La is depicted in Scheme 1.

Phosphate adsorption experiments

The adsorption experiments of phosphate were carried out according to the traditional bottle-point method [22]. The stock solution of phosphate (1000 mg L^{-1}) was prepared by dissolving certain amount of potassium dihydrogenophosphate (KH_2PO_4) powders in distilled water. The working solutions containing different concentrations of phosphate were freshly prepared by diluting the $P(PO_4^{3-})$ stock solution with distilled water. The solution pH value was adjusted to desired value with NaOH or HCl (0.1 M) solutions throughout each experiment. At the end of adsorption period, the suspensions were filtered through a 0.45-μm filter, and then, the concentrations of phosphate in the solutions were determined by UV–Vis spectrometer. All experimental data were the average of duplicate determinations. The amount of phosphate adsorbed per unit weight of adsorbent q_e (mg g^{-1}) was calculated by the following expression:

$$q_e = (C_0 - C_e)V/_m \quad (1)$$

where C_0 (mg L^{-1}) is the initial concentration of phosphate; C_e (mg L^{-1}) is the equilibrium concentration of phosphate in solution; V (mL) is the solution volume; and m (g) is the weight of the used adsorbent mass.

Adsorption isotherm

Adsorption isotherm experiments for MWCNTs-COOH-La were examined with different initial phosphate concentrations (5, 10, 20, 25, 30, 40 and 50 mg P L^{-1}) at 25 °C.

Adsorption kinetics

Adsorption kinetic experiments for MWCNTs-COOH-La were performed by using different initial concentrations (10, 20 and 50 mg P L^{-1}) at 25 °C with pH 6.0 ± 0.2. After a specific time interval (1, 3, 5, 10, 20, 30, 60, 120, 240, 360 and 480 min), approximately 1.0–2.0 mL supernatant was sampled from the reactors for the analysis of phosphate concentrations.

Effect of temperature

The effect of temperature was investigated by using 50 mg L^{-1} initial phosphate concentration at different temperatures (25, 35 and 45 °C).

Effect of pH

A series of Teflon-lined screw capped glass tubes containing 25 mg of MWCNTs-COOH-La and 40 mL of 50 mg P L^{-1} phosphate solution with different initial pH values, ranging from 3.0 to 10.0, and stirred in an orbital shaker at 25 °C.

Effect of ionic strength

Different concentrations of NaCl solution (0.01 and 0.1 mol L^{-1}) were used to investigate the effect of ionic strength on adsorption of phosphate at 25 °C under initial concentration of 50 mg L^{-1} phosphate solutions.

Effect of coexisting anions

Four typical coexisting anions (NO_3^-, SO_4^{2-}, CO_3^{2-} and HCO_3^-) with concentrations of 200 and 500 mg L^{-1} separately were also investigated at 25 °C under an initial concentration of 50 mg L^{-1} phosphate solutions.

Adsorbent characterization

The surface chemical composition and bonding structures of samples were tested by XPS, and binding energies were calibrated with respect to C–(C, H) component of the C 1s peak at 284.8 eV. The C, O, La and P were focused in this work. The specific surface area and total pore volume were determined by Nitrogen adsorption–desorption test at −196 °C on a surface area and porosity analyzer (Quantachrome Nova station A). The pore size distribution was calculated by using Barrett–Joyner–Halenda (BJH) applied to the adsorption branch of isotherm. The FTIR spectra (KBr pellet) of samples were recorded on a Model PerkinElmer 1100 series operating from 4000 to 400 cm^{-1}. Power X-ray diffraction (XRD) patterns with Cu Kα radiation were employed to investigate the crystallographic phases of samples in the 2θ range of 10°–80°. The samples were characterized with a Hitachi S-4800 field emission scanning electron microscope (SEM) coupled with an energy-dispersive spectroscopy (EDS) detector. Thermogravimetric analysis (TGA) of samples were conducted in the temperature range of 30–800 °C in N_2 atmosphere on a TA SDT Q600 apparatus, and a temperature change was 20 °C min^{-1}.

Results and discussion

The MWCNTs-COOH properties

Carboxylated multi-walled carbon nanotubes, used as raw material in the present study, were defined as "MWCNTs-COOH." Compared with MWCNTs, MWCNTs-COOH contained more oxygen groups. The main properties are listed in Table 1 (Purity >98 wt%; –COOH content 1.23 wt%; Length 10–30 μm; SSA >110 m^2 g^{-1}; Tap density 0.28 g cm^{-3}; True density ~2.1 g cm^{-3}). It was noticeable that the richness of carboxyl (–COOH) could maintain the suspensibility of MWCNTs-COOH in aqueous solution and was conducive to the adhesion of $La(OH)_3$ particles on the wall of MWCNTs-COOH through the hydrogen bonding [27] or coordination [23], which was favorable to prepare $La(OH)_3$-modified MWCNTs-COOH-La composite.

The adsorbent MWCNTs-COOH-La properties and characterizations

SEM imaging was used to test the surface morphology of MWCNTs-COOH and synthesized MWCNTs-COOH-La adsorbent. Representative images are

shown in Fig. 1. As shown in Fig. 1a, the surface of the MWCNTs-COOH appeared smooth. After La loading, there was a layer of rod-like nanoparticles on the surface of the MWCNTs-COOH, which indicated that the lanthanum was successfully coated on the surface of MWCNTs-COOH. Corresponding EDS spectrums of the MWCNTs-COOH and MWCNTs-COOH-La are also shown in Fig. 1c, d, respectively. The results revealed the presence of C, O and La in MWCNTs-COOH-La specimen. It confirmed that lanthanum was integrated successfully and distributed into the MWCNTs-COOH matrix.

FTIR. The result is shown in Fig. 3A. In Fig. 3A(a), the structure of MWCNTs-COOH was obviously observed that the peak at 1644 cm^{-1} could be assigned to the C=C stretching and the peak at 2981 cm^{-1} could be assigned to symmetric $-CH_2$ stretching. It is notable that the peaks at 1044 and 3441 cm^{-1} could be assigned to C–O and O–H stretching vibrations of the –COOH group [32]. Most importantly, the emerging peaks appeared at 3610 and 635 cm^{-1} after La loading [Fig. 3A(b)] were assigned to stretching and bending O–H vibrations of $La(OH)_3$, respectively [3]. This suggested that La species should be presented in the form of $La(OH)_3$ on the MWCNTs-COOH, apart from the loading into MWCNTs-COOH interlayer as aforementioned.

Figure 3B shows the XRD patterns of MWCNTs-COOH and MWCNTs-COOH-La. The MWCNTs-COOH [Fig. 3B(a)] exhibited the typical diffraction peaks at $2\theta = 25.9$ and 42.8, corresponding to the (002) and (100), (201) reflections of graphite phase (JCPDS card no. 41-1487) [33]. Figure 3B(b) shows that the XRD pattern of MWCNTs-COOH-La matches well with the standard cubic phase of $La(OH)_3$ including the six peaks (2θ) = 15.5, 28.1, 39.4, 48.6, 55.2 and 64.7 corresponding to the (100), (101), (201), (300), (211) and (112) reflections of $La(OH)_3$ (JCPDS card no. 83-2034), respectively [3]. These results supported the existence of $La(OH)_3$ on the MWCNTs-COOH, which were in good agreement with the FTIR results.

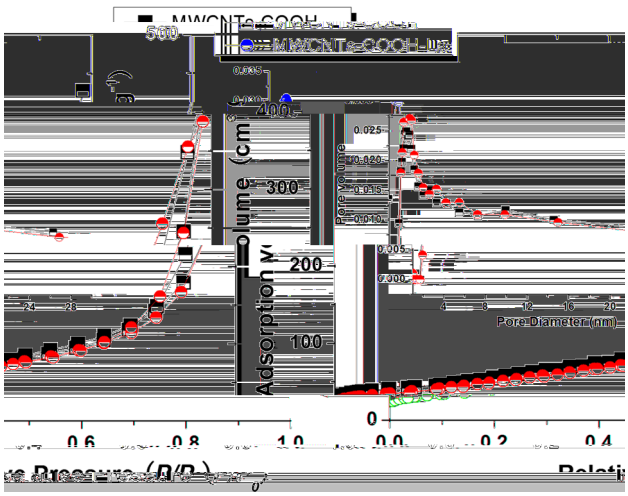

Figure 2 BET adsorption–desorption isotherms and pore volume distribution (inset) of MWCNTs-COOH and MWCNTs-COOH-La.

The effective loading form of La species was further verified by XPS analysis, and the results are presented in Fig. 3C. The survey XPS spectrum of MWCNTs-COOH exhibited signals of carbon and oxygen species. After La covering, two novel peaks appeared at around 836.7 and 853.5 eV with spin–orbit splitting of 16.8 eV, attributed to La3d5/2 and La3d3/2, respectively [34]. Additionally, the element contents of O and La increased from 0 and 2.3%, to 2.3 and 9.0% in MWCNTs-COOH-La, respectively [Fig. 3C (inset)]. It can be observed that the O and La were increased by 6.7 and 2.3%, respectively. The increased atomic ratio O/La ($^{6.7\%}/_{2.3\%} = 2.91$) was equal close to 3.0. It was speculated that $La(OH)_3$ was formed involved in the loading reaction ($La^{3+} + OH^- \overset{Basic}{\rightarrow} La(OH_3)$), which agreed with the results of FTIR and XRD analysis. With the results, it is confirmed that the surface of MWCNTs-COOH had been covered by $La(OH)_3$.

Thermal properties of MWCNTs-COOH and MWCNTs-COOH-La are presented in Fig. 3D. As for MWCNTs-COOH, the initial slight weight loss (1.0 wt%) was associated with the evaporation of water. It was known that MWCNTs decomposed lose less than 1.0 wt% of mass at around 800 °C under nitrogen. However, MWCNTs-COOH displayed a high lose about 13 wt% and this was maybe due to the introduction of –COOH units onto the surface of MWCNTs. Meanwhile, it was found the total weight loss was estimated to be 7.0 wt%, which indicated that the adsorbent MWCNT-COOH-La exhibited excellent thermal stability.

Based on the above analysis of morphology, structure and chemical composition, it was clearly

Table 2 Pore structure parameters of MWCNTs-COOH and MWCNTs-COOH-La

Samples	S_{BET} (m^2 g^{-1})	d (nm)	V_{total} (cm^3 g^{-1})[a]	La (wt%)[b]
MWCNTs-COOH	167	2.672	0.66	0
MWCNTs-COOH-La	140	2.638	0.60	7.71

[a] Total pore volume, determined at $P/P_0 = 0.98255$

[b] Calculated by the EDS results

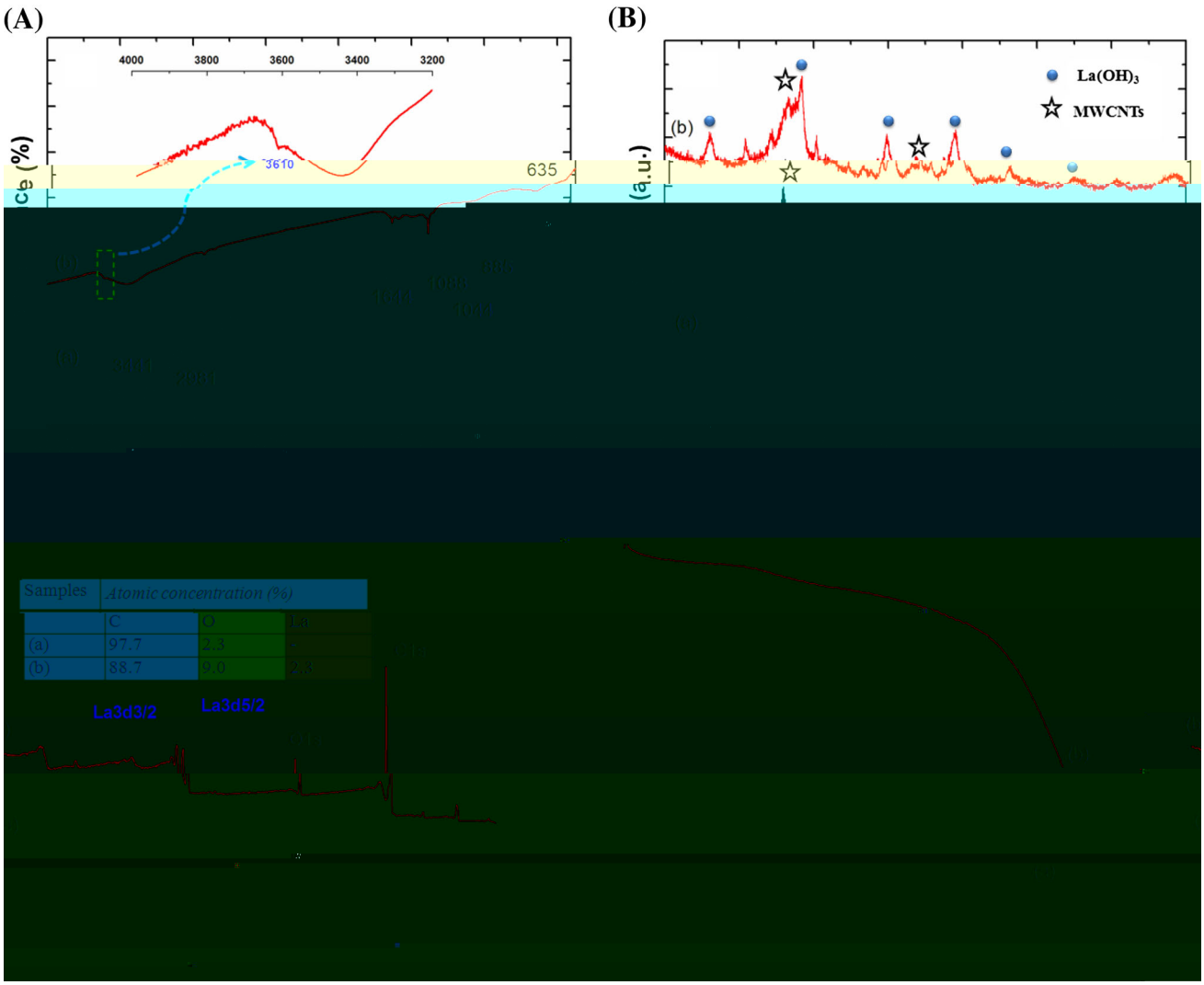

Figure 3 FTIR (**A**), XRD (**B**), XPS (**C**) and TGA spectra (**D**) of MWCNTs-COOH (a) and MWCNTs-COOH-La (b), respectively.

that the $La(OH)_3$ was formed and successfully loaded on the MWCNTs-COOH matrix, which could act as active species for phosphate anions adsorption.

Phosphate adsorption

Adsorption isotherms

Adsorption isotherms studies were performed to investigate the maximum uptake capacity of phosphate on the adsorbent MWCNTs-COOH-La. Figure 4 shows the fittings of phosphate adsorption data of MWCNTs-COOH-La at 25 °C into the Langmuir [Eq. (2)] Freundlich [Eq. (3)] and Temkin [Eq. (4)] adsorption isotherms [35], respectively. The relevant values of adsorption parameters and regression coefficients (R^2 value) are summarized in Table 3.

The three equations can be expressed as:Langmuir model:

$$q_e = \frac{q_m b C_e}{1 + b C_e} \tag{2}$$

Freundlich model:

$$q_e = K_F C_e^{1/n} \tag{3}$$

Temkin model:

$$q_e = A + B \ln C_e \tag{4}$$

where q_e (mg g^{-1}) is the amount adsorbed of phosphate per unit weight of adsorbent at equilibrium, C_e (mg L^{-1}) is the equilibrium concentration of phosphate in equilibrium, b (L mg^{-1}) is the Langmuir model constant, q_m (mg g^{-1}) is the maximum adsorption capacity, K_F is the Freundlich model

constant, 1/n is heterogeneity factor, and A and B are the Temkin model constants.

The R^2 for Langmuir, Freundlich and Temkin models were 0.950, 0.753 and 0.861, respectively. The results indicated that adsorption equilibrium data used in this study fitted better by the Langmuir model than the Freundlich model and Temkin models, which indicated that the adsorption feature onto MWCNTs-COOH-La was monolayer [36]. The result is in an agreement with those reports of other lanthanum-modified adsorbents, such as lanthanum-modified bentonite [37]. Furthermore, a dimensionless constant, called separation factor or equilibrium parameter (R_L), obtained from the Langmuir adsorption isotherm can be used to predict the affinity between the adsorbate and adsorbent [38], which was calculated by the following equation:

$$R_L = \frac{1}{1 + bC_0} \quad (5)$$

where C_o is the highest initial solute concentration. The R_L value indicates that the type of adsorption isotherm is irreversible ($R_L = 0$), favorable ($0 < R_L < 1$), linear ($R_L = 1$) or unfavorable ($R_L > 1$), respectively. The factor R_L value of MWCNTs-COOH-La was calculated to be 0.0276 which was found to be lower than 1.0, characteristic of favorable adsorption of phosphate on the MWCNTs-COOH-La [39].Most importantly, as results shown in Fig. 5, it can be seen that MWCNTs-COOH-La possessed significantly high uptake capacity for phosphate (48.02 mg P g^{-1}) estimated via the Langmuir model, as compared with unmodified MWCNTs-COOH (2.63 mg P g^{-1}). This proved that MWCNTs-COOH-La was an outstanding adsorbent for phosphate attributed to the $La(OH)_3$ loaded onto the MWCNTs-COOH, providing a large number of independent active sites for phosphate adsorption [4]. This confirmed that loading of $La(OH)_3$ was an efficient way

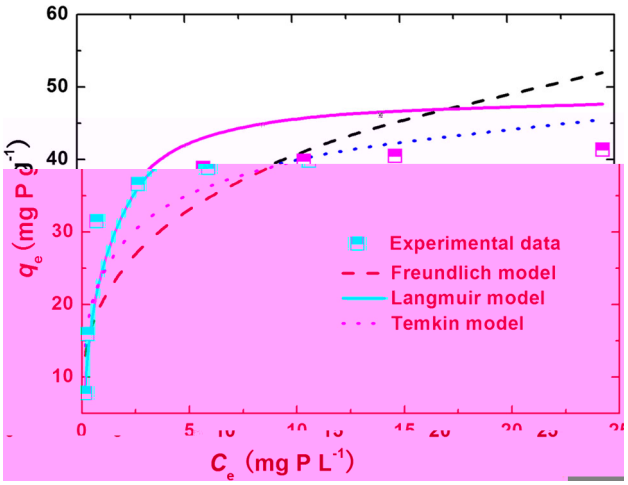

Figure 4 Langmuir, Freundlich and Temkin adsorption isotherms of MWCNTs-COOH-La with adsorbent dose at 0.625 g L^{-1}, at 25 °C.

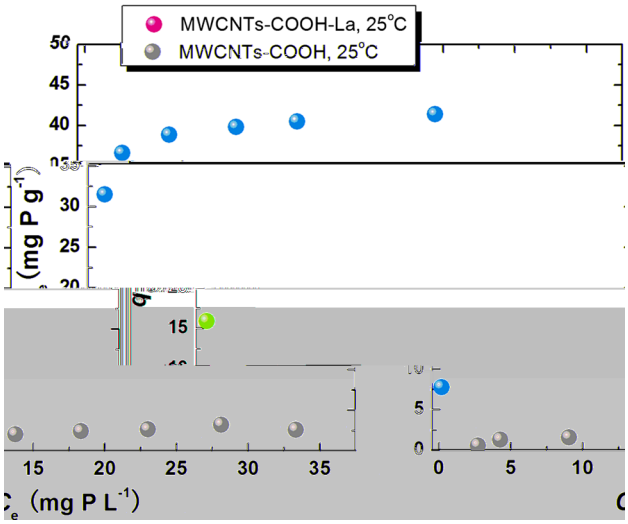

Figure 5 Adsorption isotherm of phosphate by MWCNTs-COOH-La and MWCNTs-COOH with adsorbent dose at 0.625 g L^{-1}, at 25 °C.

Table 3 Adsorption equilibrium constants obtained from Langmuir, Freundlich and Temkin isotherms, where R is the correlation coefficient with adsorbent dose at 0.625 g L^{-1}, at 25 °C

	Temperature (°C)	Langmuir isotherm constants				Freundlich isotherm constants			Temkin isotherm constants		
		b (L mg^{-1})	R_L	q_m (mg g^{-1})	R^2	K_F	n	R^2	A	B	R^2
MWCNTs-COOH-La	25	1.41	0.0276	48.02	0.950	21.77	3.67	0.753	6.124	25.94	0.861

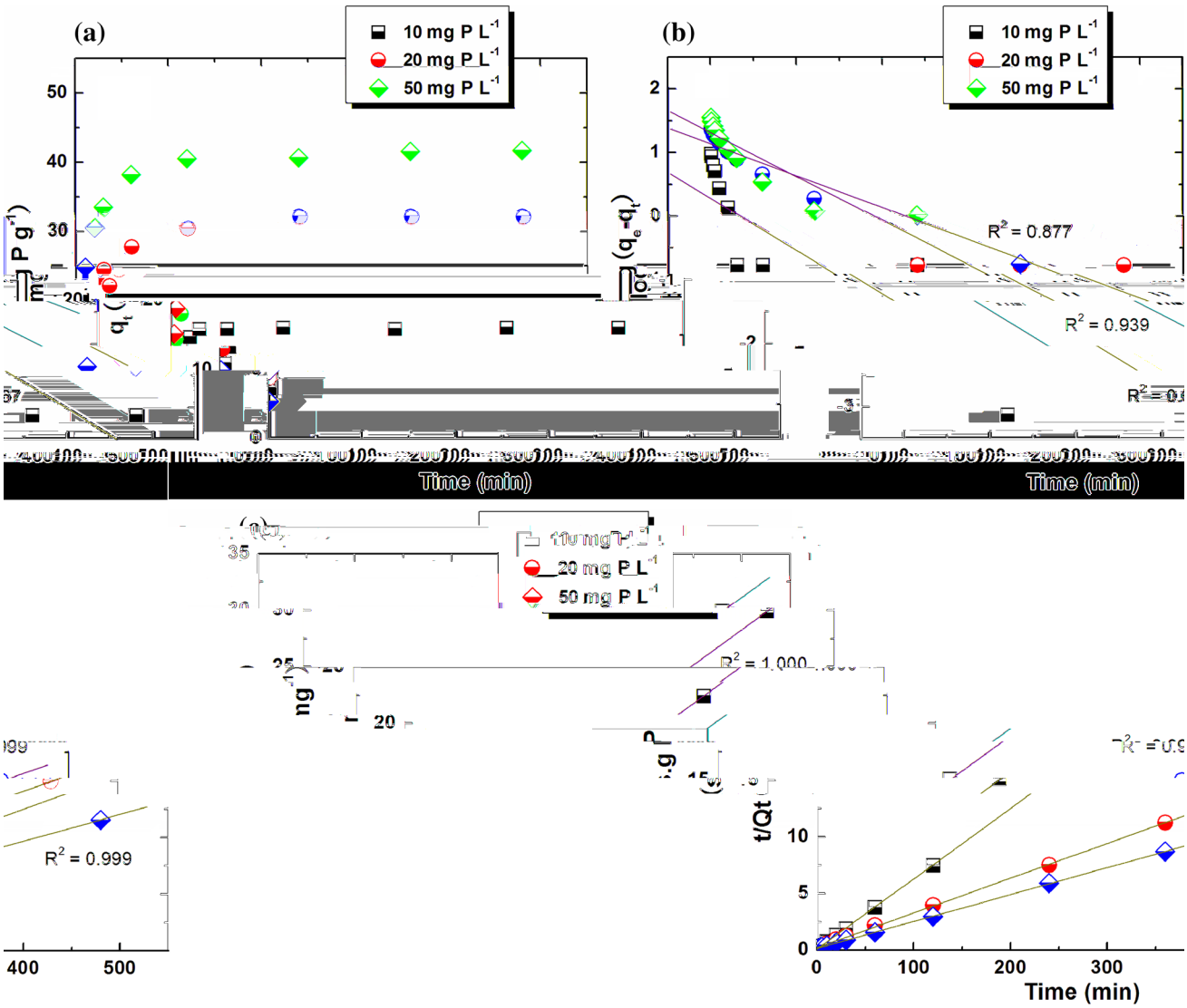

Figure 6 Effect of contact time on the phosphate adsorption of MWCNTs-COOH-La (10, 20 and 50 mg P L^{-1}) (**a**), pseudo-first-order model (**b**) and pseudo-second-order model (**c**).

in enhancing the phosphate sequestering ability of MWCNTs-COOH. Additionally, it was worth mentioning that the high adsorption capacity of the MWCNTs-COOH-La was achieved at a low equilibrium concentration (0.67 mg L^{-1}), indicating that it was more feasible for the removal of low phosphate concentration to MWCNTs-COOH-La [40].

Effect of temperature on the adsorption

Effect of temperature on the adsorption capacity of phosphate by MWCNTs-COOH-La is shown in Fig. S1. It was clearly seen that the adsorption capacity of MWCNTs-COOH-La maintained about 42.10 mg P g^{-1} when the temperature varied from 25 to 45 °C. This indicated that the equilibrium adsorption capacity was almost unaffected by temperature, and the adsorption behavior could be performed at a wide range of temperature. Similar adsorption dependency on temperature was also reported in the other lanthanum-modified adsorbents, such as lanthanum-modified mesoporous hybrid film [4], and lanthanum-modified vesuvianite [41].

Adsorption kinetics

Phosphate elimination by MWCNTs-COOH-La as a function of time with different initial concentrations (10, 20 and 50 mg P L^{-1}) is shown in Fig. 6a. It can be

Table 4 Kinetic parameters of pseudo-first-order, pseudo-second-order and intra-particle diffusion models for phosphate adsorption onto MWCNTs-COOH-La with different phosphate initial concentrations at 10, 20 and 50 mg P L^{-1}, respectively, adsorbent dose at 0.625 g L^{-1}, at 25 °C

C_o (mg P L^{-1})	($q_{e,\ exp}$)	Pseudo-first-order kinetics			Pseudo-second-order kinetics		
		($q_{e,\ cal}$) (mg P g^{-1})	k_1 (g mg^{-1} min^{-1})	R^2	($q_{e,\ cal}$) (mg P g^{-1})	k_2 (g mg^{-1} min^{-1})	R^2
10	16.05	1.88	0.0189	0.6708	16.10	0.0433	1.0000
20	32.13	13.65	0.0115	0.8777	32.57	0.0048	0.9996
50	42.50	20.67	0.0159	0.9392	42.19	0.0040	0.9999

	Intra-particle diffusion model					
	C_1 (mg P g^{-1})	k_{d1} (mg P g^{-1} $min^{-1/2}$)	R_1^2	C_2 (mg P g^{-1})	k_{d2} (mg P g^{-1} $min^{-1/2}$)	R_2^2
10	0	7.359	1	7.413	1.610	0.961
20	0	9.742	1	7.687	3.143	0.994
50	0	9.979	1	7.896	4.848	0.977

seen that the adsorption capacity increased from 16.05 mg P g^{-1} in 10 mg P L^{-1} solution to 42.50 mg P g^{-1} in 50 mg P L^{-1} solution, which was due to higher driving force provided by higher concentration. Additionally, the phosphate uptake capacity increased with an increase in contact time.

In order to assess the adsorption efficiency of MWCNTs-COOH-La and understand the diffusion mechanism involved during the whole adsorption process, the adsorption kinetic was investigated using various kinetic equations. The best popular equation is the pseudo-first-order model [Eq. (6)] [42]. It can be expressed as below

$$\log(q_e - q_t) = \log q_e - \frac{k_1 t}{2.303} \quad (6)$$

The integral form of the pseudo-second-order model is given by the following expressions.

$$\frac{t}{q_t} = \frac{1}{k_2 q_e^2} + \frac{t}{q_e} \quad (7)$$

where q_e and q_t (mg g^{-1}) denote the adsorbed amount (mg g^{-1}) at equilibrium and at time t, respectively. The values of the pseudo-first-order model rate constant k_1 (g mg^{-1} min^{-1}) can be obtained from the slope of the linear $\log(q_e - q_t)$ against t of different concentrations of phosphate, and the values of the pseudo-second-order model rate constant k_2 (g mg^{-1} min^{-1}) can be calculated from the plots of (t/q_t) against t.

The linear plots of phosphate adsorption kinetics to pseudo-first-order model and pseudo-second-order model are shown in Fig. 6b, c, respectively. Table 4 gave the fitted kinetic parameters determined from the first-order kinetic model and the second-order kinetic model. It was clearly found that the theoretical ($q_{e,\ cal}$) values determined from the pseudo-second-order model were in better agreement with corresponding experimental values ($q_{e,\ exp}$), and meanwhile, the correlation coefficients ($R^2 > 0.999$) were observed to be higher, meaning that the adsorption system of the MWCNTs-COOH-La belonged to the second-order kinetic model. Thereby, it is confirmed that the adsorption for phosphate onto MWCNTs-COOH-La was responsible for the chemisorption. Moreover, the rate constants (k_2) decreased from 0.0433 to 0.0040 g mg^{-1} min^{-1} with increasing initial concentrations from 10 to 50 mg P L^{-1} indicating of more favorable adsorption behavior at low concentrations to MWCNTs-COOH-La [17].

It is generally known that the adsorption process is a multi-step process which follows external diffusion, intra-particle diffusion and adsorption before reaching equilibrium state. In order to investigate the dominating step of adsorption, the intra-particle diffusion model [Eq (8)] was taken into account. The intra-particle diffusion model according to the theory proposed by Weber and Morris [43] is given as:

$$q_t = k_{di}\sqrt{t} + c_i \quad (8)$$

Values of the intra-particle diffusion rate constant k_{di} (mg g^{-1} $min^{-1/2}$) and c_i (mg g^{-1}) are calculated from the slope of the linear plot of q_t against $t^{1/2}$ and intercept of stage i. Fig. S2a presents the variation of phosphate adsorption capacity as a function of $t^{1/2}$ with different initial concentrations (10, 20 and

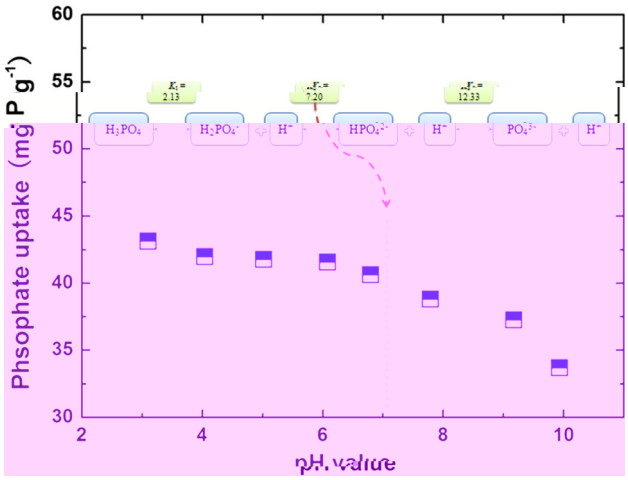

Figure 7 Effect of pH value on phosphate adsorption with the initial phosphate concentration at 50 mg L^{-1}, adsorbent dose at 0.625 g L^{-1}, at 25 °C.

50 mg P L^{-1}). The intra-particle plots for phosphate adsorption onto MWCNTs-COOH-La at different initial phosphate concentrations are shown in Fig.S2b–d, respectively. Table 4 gave the rate parameters for intra-particular diffusion model. It can be seen that the plots were not linear over the entire contact time and mainly consist of three linear portions, indicative of multi-step process of phosphate adsorption to MWCNTs-COOH-La. In the first step, the fast adsorption rate might be attributed to either external surface adsorption or layer diffusion of the MWCNTs-COOH-La, since the richness of binding sites was available for adsorption [44]. The second linear portion was the gradual adsorption stage where intra-particle diffusion or pore diffusion was the rate limiting step, which was evidenced by the lower values of the rate constants (1.61, 3.14 and 4.85 mg P g^{-1} $min^{-1/2}$) than the rate constants of the first stage (7.36, 9.74 and 9.98 mg P g^{-1} $min^{-1/2}$) under the same initial phosphate concentration. The third portion was final equilibrium stage. Additionally, the values of correlation coefficients ($R^2 > 0.96$) for the first and second steps were all high and the lines in the second step did not pass through origin, which indicated that the phosphate adsorption might be mainly controlled by the intra-particle diffusion [45].

Effect of pH value on phosphate adsorption

Generally, the adsorption was influenced by the solution pH value. Thus, effect of solution pH on phosphate uptake by MWCNTs-COOH-La was also examined in our study. The results are illustrated in Fig. 7. It could be seen that the adsorption process of phosphate was strongly dependent on the pH value of solution. The adsorption capacity of MWCNTs-COOH-La changed very little within the pH range of 3.0–7.0. As pH reached 10.0, the adsorption capacity of MWCNTs-COOH-La (33.7 mg P g^{-1}) was reduced by 22%, as compared with the value at pH 3.0 (43.1 mg P g^{-1}). The species of phosphate was different when the pH changed from 3.0 to 10.0, as expressed in the equations [Fig. 7 (inset)]. Thus, the main species is monovalent dihydrogen phosphate in the aqueous solution when the pH value is between 2.13 and 7.20, indicating that MWCNTs-COOH-La provided a great affinity to the single-charged phosphate species ($H_2PO_4^-$). When the pH value increased from 7.20 to 10.0, the predominant forms of phosphate species were hydrogen phosphate (HPO_4^{2-}). Therefore, as the pH increased, the surface of adsorbent became more negative and repelled phosphate ions (PO_4^{3-}, HPO_4^{2-} and $H_2PO_4^-$) [21]. Another contribution to poorer adsorption capacity at higher pH was likely due to the competition of phosphate with hydroxyl groups [30, 46]. Thus, low adsorption capacity of MWCNTs-COOH-La was observed in the pH value range of 7.0–10.0.

Effect of ionic strength on phosphate adsorption

The effect of ionic strength was studied at room temperature, and the results are shown in Fig.S3. It was found that a slight variety in phosphate adsorption with increasing the NaCl concentration from 0 to 0.1 M. These results might be because that Cl^- ion possessed poor affinity toward the adsorption sites of the MWCNTs-COOH-La compared with P(PO_4^{3-}), and no visible competition between Cl^- and P(PO_4^{3-}) for the adsorption sites was observed. It was worth pointing out that the adsorption capacity onto MWCNTs-COOH-La was virtually uninfluenced by the increasing ionic strength, indicative of an inner-sphere complex adsorption mechanism to MWCNTs-COOH-La [47].

Effect of coexisting anions on phosphate adsorption

Considering that the phosphate-contaminated water usually includes some coexisting anions, the competitive adsorption for the active sites on the adsorbent was investigated between P(PO_4^{3-}) and nitrate (NO_3^-), sulfate (SO_4^{2-}), carbonate (CO_3^{2-}), bicarbonate

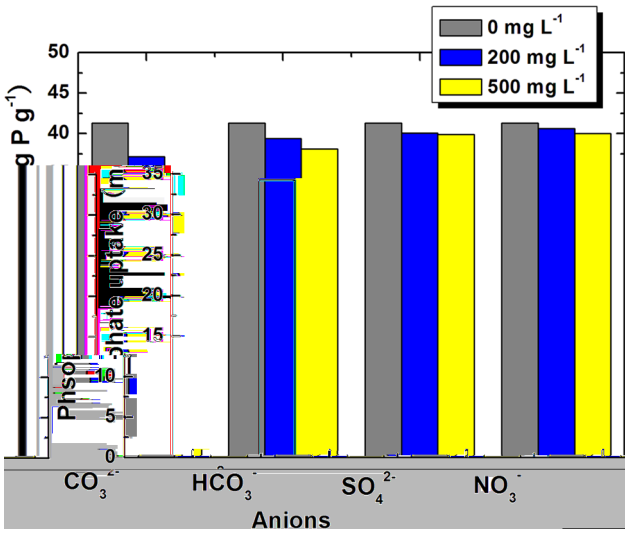

Figure 8 Effects of coexisting anions on phosphate adsorption capacity on the MWCNTs-COOH-La with the initial phosphate concentration at 50 mg L^{-1}, adsorbent dose at 0.625 g L^{-1}, at 25 °C.

(HCO_3^-) [47]. The adsorption experiments were performed in the presence of 200 and 500 mg L^{-1} solutions of NO_3^-, SO_4^{2-}, CO_3^{2-} and HCO_3^-, respectively. The results are presented in Fig. 8. The phosphate adsorption capacity of MWCNTs-COOH-La in the absence of competitive anions was 42.10 mg P g^{-1}. However, as shown in Fig. 8, it was found that the phosphate adsorption was remarkly reduced to 34.15 mg g^{-1} when CO_3^{2-} concentration was increased to 500 mg L^{-1}. Similar adsorption dependency on coexisting anions was also reported in the literature [13]. This was maybe attributed to the lower solubility product constant (K_{sp}) of $La_2(CO_3)_3$ (3.98×10^{-34}) compared with that of $LaPO_4$ (3.7×10^{-23}), which supported the alteration of the formed $LaPO_4$ to $La_2(CO_3)_3$ [48]. On the other hand, the initial pH of the CO_3^{2-}solution with 500 mg L^{-1} was expected to be highest among these tested anions due to the largest hydrolysis constant, which led to the lowest adsorption capacity. Additionally, no obvious change was observed when NO_3^-, SO_4^{2-} and HCO_3^- anions were incorporated. That was to say, MWCNTs-COOH-La still possessed a high selectivity to phosphate.

Characterization before and after phosphate adsorption

To investigate the adsorption mechanism, XRD, FTIR and XPS technologies were employed and the structure characteristics of the adsorbent before and after phosphate adsorption were analyzed. The material after phosphate adsorption is denoted as MWCNTs-COOH-La-P.

Figure 9a shows the XRD patterns of MWCNTs-COOH-La and MWCNTs-COOH-La-P, respectively. After $P(PO_4^{3-})$ adsorption on MWCNTs-COOH-La, characteristic peaks for $La(OH)_3$ decreased. Meanwhile, several new characteristic peaks appeared at $2\theta = 14.7$, 20.2, 25.0, 28.8, 31.2, 41.9 and 48.2 in MWCNTs-COOH-La-P [3], which corresponded to the monoclinic $LaPO_4$ phase (PDF no.73-0188), confirming that the adsorbed $P(PO_4^{3-})$ had reacted with La active sites [22]. With these results, it could be concluded that lanthanum phosphate was formed on MWCNTs-COOH-La during the adsorption process.

Figure 9b shows the FTIR spectrum of MWCNTs-COOH-La and MWCNTs-COOH-La-P. Most importantly, the two bands centered at 3610 and 635 cm^{-1} assigned to surface hydroxyl groups of MWCNTs-COOH-La completely disappeared after the adsorption of phosphate at 50 mg L^{-1}. The changes in these two peaks after adsorption aroused from the release of surface hydroxyls into the solution. Meanwhile, two additional adsorption peaks centered at 1052 and 1004 cm^{-1} were attributed to HPO_4^{2-} and $H_2PO_4^-$ groups, respectively [49]. Additionally, the appearance of the O–P–O peak at 615 and 532 cm^{-1} also suggested the chemical binding between La and $P(PO_4^{3-})$ [3, 50], indicating that the replacement of hydroxyl groups occurred during the phosphate adsorption process. These results further verified the involvement of surface hydroxyl group in the adsorption of $P(PO_4^{3-})$.

To further illustrate the adsorption mechanism of $P(PO_4^{3-})$ on the MWCNTs-COOH-La, the compositions and chemical states of MWCNTs-COOH-La and MWCNTs-COOH-La-P were revealed by XPS analysis. P2p spectrum of MWCNTs-COOH-La-P can be fitted to the peak at 134.8 eV [Fig. 9d], indicative of the existence of sole type of phosphorus compounds in the structure which derived from the $P(PO_4^{3-})$. It was reported that P2p binding energy for Na_2HPO_4 was 133.1 eV [51]. The higher binding energy of P2p at 134.8 eV was because that the surface adsorption or coordination reactions had occurred between $P(PO_4^{3-})$ and La. Additionally, La3d spectra of the MWCNTs-COOH-La and MWCNTs-COOH-La-P are displayed in Fig. 9c. It was important to notice that the main peaks of La3d changed and shifted to higher

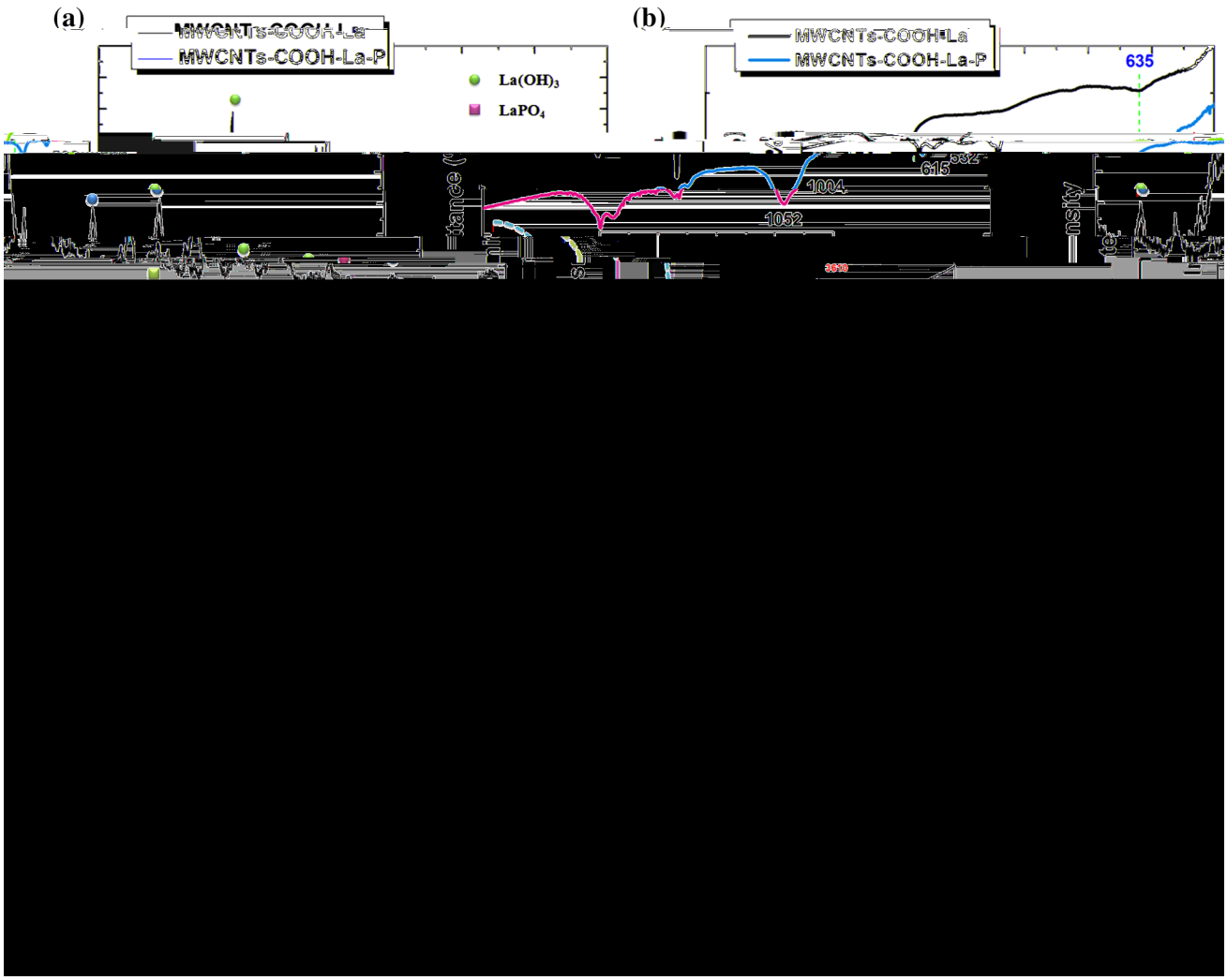

Figure 9 XRD (**a**), FTIR (**b**) and XPS spectra of La in the MWCNTs-COOH-La (**c**) before and after adsorption (MWCNTs-COOH-La-P) and P 2p XPS scan spectrum of MWCNTs-COOH-La-P (**d**).

binding energy 837.3 and 854.1 eV (0.6 eV), demonstrating that hydroxyl groups were displaced by phosphate anion and the new La species (La–O–P) was formed after absorption. Moreover, a decrease in La3d spectra intensity was also observed after reaction with $P(PO_4^{3-})$. These results indicated that hydroxyl groups bonded to La species were involved in the adsorption of $P(PO_4^{3-})$ [52].

Based on the above experimental results, the mechanism of $P(PO_4^{3-})$ adsorption on MWCNTs-COOH-La occurred possibly via a ligand exchange, which was also confirmed by the literature [24]. Within the experiment solution pH of 6.0 ± 0.2, $La(OH)_2^+$ was the dominant La species [48, 53] and the phosphate specie existed mainly as $H_2PO_4^-$. MWCNTs-COOH could capture $La(OH)_2^+$, and it formed the MWCNTs-COO^- $[La(OH)_2^+]$ composite [19] (reaction 1). Afterward, one or two $H_2PO_4^-$ molecules approached the active sites of MWCNTs-COO^- $[La(OH)_2^+]$, which would further exchange with the surface of hydroxyl groups (reaction 2) and then form a monodentate complex or an adjacent monodentate complex [24]. The adsorption mechanism of phosphate on MWCNTs-COOH-La is depicted in Scheme 2 [53, 54].

Comparison with other adsorbents

To assess the potential in the use of the MWCNTs-COOH-La as an adsorbent for phosphate, a comparative evaluation of the adsorption capacities of some

Scheme 2 Schematic mechanism of MWCNTs-COOH-La adsorption.

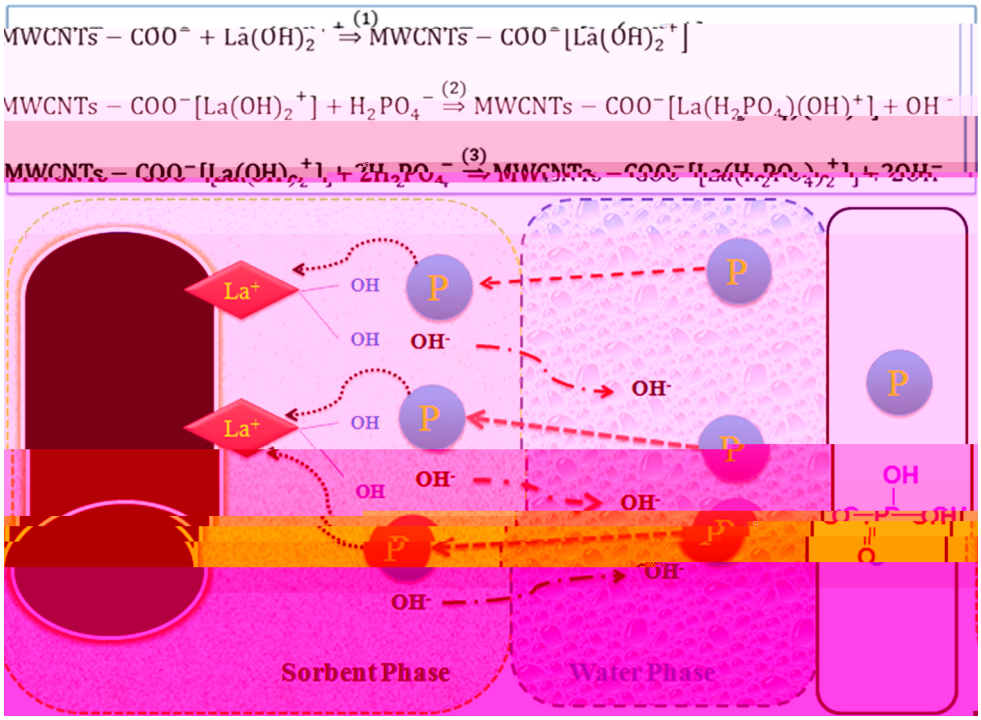

Table 5 Comparison of phosphate adsorption capacities between the adsorbent (MWCNTs-COOH-La) and other different lanthanum-modified composites in literatures

Absorbents	Initial concentration of phosphate (mg P L^{-1})	pH values	Phosphate adsorption capacities (mg P g^{-1})	References
Lanthanum-modified activated carbon fiber	10–70	–	15.3	Zhang et al. [20]
Lanthanum-modified bentonite	–	–	14.0	Kuroki et al. [37]
Lanthanum-modified exfoliated vermiculites	1–100	5	79.6	Huang et al. [30]
Lanthanum-modified zeolite	–	6.0	24.6	Ning et al. [55]
Lanthanum-modified aluminum pillared montmorillonite	–	5.0	13.02	Tian et al. [56]
Lanthanum-modified mesoporous hybrid film	–	4.0	42.7	Zheng et al. [4]
Lanthanum-modified vesuvianite	1–5	7.1	1.32	Li et al. [41]
Lanthanum-modified chelex resin	5 mM	5.5	8.74	Wu et al. [23]
Lanthanum-modified graphene	14–292	6.2	82.6	Chen et al. [57]
Lanthanum-modified granular ceramic	10	7	0.89	Chen et al. [54]
Lanthanum-modified carboxylated multi-walled carbon nanotubes	10–50	6	48.02[a]	This study

[a] Calculated from the Langmuir isotherm model

lanthanum-modified composites [4, 20, 23, 30, 37, 41, 54–57] for the phosphate adsorption is summarized in Table 5. The adsorption capacity of MWCNTs-COOH-La revealed its higher adsorption performance for phosphate than most adsorbents, except for lanthanum-modified exfoliated vermiculites and lanthanum-modified graphene. Lanthanum-modified exfoliated vermiculites performed around 1.6 times better than MWCNTs-COOH-La under the same initial concentration of 50 mg P L^{-1}. Nevertheless, it is worth pointing out that lanthanum-modified exfoliated vermiculites adsorption result was achieved with a long contact time (24 h) and it possessed a high La content (31.52 wt%). The lanthanum-modified graphene showed around 1.7 times adsorption capacity of MWCNTs-COOH-La;

this was mainly attributed to a high initial concentration (292 mg P L^{-1}). The results evidenced that MWCNTs-COOH-La still should be a highly effective adsorbent for remediating phosphate from aqueous solution.

Conclusions

In summary, a novel MWCNTs-COOH-La adsorbent was successfully prepared via a simple codeposition-precipitation method and employed for phosphate adsorption. Most importantly, MWCNTs-COOH-La possessed significantly high uptake capacity for phosphate (48.02 mg P g^{-1}) according to the Langmuir model, as compared with unmodified MWCNTs-COOH (2.63 mg P g^{-1}). The experimental data could be well described by the pseudo-second-order equation, suggesting it was chemic-sorption. The adsorption isotherms followed the Langmuir model, indicative of a monolayer adsorption. The acidic condition was favorable for the adsorption. Solution pH was a vital factor influencing the phosphate adsorption capacity and it decreased with the increasing pH. The presence of 200 or 500 mg L^{-1} competing ions slightly affected phosphate adsorption capacity, while the CO_3^{2-} suppressed its adsorption, especially at high concentration level. The adsorption capacity was almost uninfluenced with increasing the background ionic strength from 0 to 0.1 M. The La species was presented in the form of $La(OH)_3$ on the MWCNTs-COOH, the phosphate adsorption possible mainly completed by substituting phosphate species with surface of hydroxyl groups, and the formation of $LaPO_4$ was a pathway for phosphate adsorption, as demonstrated by XRD, FTIR and XPS. Our results showed that the $La(OH)_3$-modified MWCNTs-COOH was a promising adsorbent for the effective removal of phosphate from aqueous solution.

Acknowledgement

We greatly acknowledge the financial support from the Special Fund for the Ecology Key Disciplines of Zhejiang Province in Taizhou University, Jiangsu Key Lab. of Biomass Energy and Material Foundation of China (JSBEM201703), the Program for key Science and Technology Team of Zhejiang Province (2013TD17), and the Program for Zhejiang Provincial Natural Science Foundation of China (LZ16C160001).

Electronic supplementary material: The online version of this article (doi:10.1007/s10853-017-0966-0) contains supplementary material, which is available to authorized users.

References

[1] Zhang W, Jin X, Zhu X, Shan B (2016) Characteristics and distribution of phosphorus in surface sediments of limnetic ecosystem in eastern China. PLoS one 11(6):e0156488. doi:10.1371/journal.pone.0156488

[2] Arshadi M, Zandi H, Akbari J, Shameli A (2015) Ferrocene functionalized nanoscale mixed-oxides as a potent phosphate adsorbent from the synthetic and real (Persian Gulf) waters. J Colloid Interface Sci 450:424–433

[3] He J, Wang W, Sun F, Shi W, Qi D, Wang K, Shi R, Cui F, Wang C, Chen X (2015) Highly efficient phosphate scavenger based on well-dispersed $La(OH)_3$ nanorods in polyacrylonitrile nanofibers for nutrient-starvation antibacteria. ACS Nano 9(9):9292–9302

[4] Zheng X, Pan J, Zhang F, Liu E, Shi W, Yan Y (2016) Fabrication of free-standing bio-template mesoporous hybrid film for high and selective phosphate removal. Chem Eng J 284:879–887. doi:10.1016/j.cej.2015.09.033

[5] Rodrigues LA, da Silva MLCP (2010) Thermodynamic and kinetic investigations of phosphate adsorption onto hydrous niobium oxide prepared by homogeneous solution method. Desalination 263(1–3):29–35

[6] Liu X, Zhang L (2015) Removal of phosphate anions using the modified chitosan beads: adsorption kinetic, isotherm and mechanism studies. Powder Technol 277:112–119

[7] Benyoucef S, Amrani M (2011) Adsorption of phosphate ions onto low cost Aleppo pine adsorbent. Desalination 275(1):231–236

[8] Ju X, Hou J, Tang Y, Sun Y, Zheng S, Xu Z (2016) ZrO_2 nanoparticles confined in CMK-3 as highly effective sorbent for phosphate adsorption. Microporous Mesoporous Mater 230:188–195

[9] Lürling M, Fv Oosterhout (2013) Controlling eutrophication by combined bloom precipitation and sediment phosphorus inactivation. Water Res 47(17):6527–6537

[10] Eggers E, Dirkzwager A, Van der Honing H (1991) Full-scale experiences with phosphate crystallization in a Crystalactor®. Water Sci Technol 23(4–6):819–824

[11] Chen L, Zhao X, Pan B, Zhang W, Hua M, Lv L, Zhang W (2015) Preferable removal of phosphate from water using hydrous zirconium oxide-based nanocomposite of high stability. J Hazard Mater 284:35–42

[12] Jabari P, Munz G, Yuan Q, Oleszkiewicz JA (2016) Free nitrous acid inhibition of biological phosphorus removal in integrated fixed-film activated sludge (IFAS) system. Chem Eng J 287:38–46

[13] Huang W, Yu X, Tang J, Zhu Y, Zhang Y, Li D (2015) Enhanced adsorption of phosphate by flower-like mesoporous silica spheres loaded with lanthanum. Microporous Mesoporous Mater 217:225–232

[14] Khodadadi Dizaji A, Mortaheb HR, Mokhtarani B (2016) Noncovalently functionalized graphene oxide/graphene with imidazolium-based ionic liquids for adsorptive removal of dibenzothiophene from model fuel. J Mater Sci 51(22):10092–10103. doi:10.1007/s10853-016-0237-5

[15] Huang Q, Liu M, Guo R, Mao L, Wan Q, Zeng G, Huang H, Deng F, Zhang X, Wei Y (2016) Facile synthesis and characterization of poly(levodopa)-modified silica nanocomposites via self-polymerization of levodopa and their adsorption behavior toward Cu2+. J Mater Sci 51(21):9625–9637. doi:10.1007/s10853-016-0178-z

[16] Shakur HR, Rezaee Ebrahim Saraee K, Abdi MR, Azimi G (2016) A novel PAN/NaX/ZnO nanocomposite absorbent: synthesis, characterization, removal of uranium anionic species from contaminated water. J Mater Sci 51(22):9991–10004. doi:10.1007/s10853-016-0227-7

[17] Zong E, Wei D, Wan H, Zheng S, Xu Z, Zhu D (2013) Adsorptive removal of phosphate ions from aqueous solution using zirconia-functionalized graphite oxide. Chem Eng J 221:193–203

[18] Zong E, Liu X, Jiang J, Fu S, Chu F (2016) Preparation and characterization of zirconia-loaded lignocellulosic butanol residue as a biosorbent for phosphate removal from aqueous solution. Appl Surf Sci 387:419–430

[19] Cui G, Liu M, Chen Y, Zhang W, Zhao J (2016) Synthesis of a ferric hydroxide-coated cellulose nanofiber hybrid for effective removal of phosphate from wastewater. Carbohydr Polym 154:40–47

[20] Zhang L, Zhou Q, Liu J, Chang N, Wan L, Chen J (2012) Phosphate adsorption on lanthanum hydroxide-doped activated carbon fiber. Chem Eng J 185–186:160–167

[21] Ko YG, Do T, Chun Y, Kim CH, Choi US, Kim J-Y (2016) CeO_2-covered nanofiber for highly efficient removal of phosphorus from aqueous solution. J Hazard Mater 307:91–98

[22] Zhang Y, Pan B, Shan C, Gao X (2016) Enhanced phosphate removal by nanosized hydrated La(III) oxide confined in cross-linked polystyrene networks. Environ Sci Technol 50(3):1447–1454

[23] Wu RSS, Lam KH, Lee JMN, Lau TC (2007) Removal of phosphate from water by a highly selective La(III)-chelex resin. Chemosphere 69(2):289–294

[24] Acelas NY, Martin BD, López D, Jefferson B (2015) Selective removal of phosphate from wastewater using hydrated metal oxides dispersed within anionic exchange media. Chemosphere 119:1353–1360

[25] Gupta VK, Agarwal S, Saleh TA (2011) Synthesis and characterization of alumina-coated carbon nanotubes and their application for lead removal. J Hazard Mater 185(1):17–23

[26] Saleh TA, Agarwal S, Gupta VK (2011) Synthesis of MWCNT/MnO_2 and their application for simultaneous oxidation of arsenite and sorption of arsenate. Appl Catal B 106(1–2):46–53

[27] Liang J, Liu J, Yuan X, Dong H, Zeng G, Wu H, Wang H, Liu J, Hua S, Zhang S, Yu Z, He X, He Y (2015) Facile synthesis of alumina-decorated multi-walled carbon nanotubes for simultaneous adsorption of cadmium ion and trichloroethylene. Chem Eng J 273:101–110

[28] Wang S-G, Gong W-X, Liu X-W, Yao Y-W, Gao B-Y, Yue Q-Y (2007) Removal of lead(II) from aqueous solution by adsorption onto manganese oxide-coated carbon nanotubes. Sep Purif Technol 58(1):17–23

[29] Peng X, Luan Z, Ding J, Di Z, Li Y, Tian B (2005) Ceria nanoparticles supported on carbon nanotubes for the removal of arsenate from water. Mater Lett 59(4):399–403

[30] Huang W-Y, Li D, Liu Z-Q, Tao Q, Zhu Y, Yang J, Zhang Y-M (2014) Kinetics, isotherm, thermodynamic, and adsorption mechanism studies of $La(OH)_3$-modified exfoliated vermiculites as highly efficient phosphate adsorbents. Chem Eng J 236:191–201

[31] Zong E, Wei D, Huan Z, Du P, Wan H, Zheng S, Xu Z (2013) Adsorption of phosphate by zirconia functionalized multi-walled carbon nanotubes. Chin J Inorg Chem 29(05):965–972

[32] Zhao Z, Yang Z, Hu Y, Li J, Fan X (2013) Multiple functionalization of multi-walled carbon nanotubes with carboxyl and amino groups. Appl Surf Sci 276:476–481

[33] Jiang L, Li S, Yu H, Zou Z, Hou X, Shen F, Li C, Yao X (2016) Amino and thiol modified magnetic multi-walled carbon nanotubes for the simultaneous removal of lead, zinc, and phenol from aqueous solutions. Appl Surf Sci 369:398–413

[34] Kang J-G, Kim Y-I, Won Cho D, Sohn Y (2015) Synthesis and physicochemical properties of $La(OH)_3$ and La_2O_3 nanostructures. Mater Sci Semicond Process 40:737–743

[35] Njoku VO, Foo KY, Asif M, Hameed BH (2014) Preparation of activated carbons from rambutan (Nephelium lappaceum) peel by microwave-induced KOH activation for acid yellow 17 dye adsorption. Chem Eng J 250:198–204

[36] Tang J, Chen J, Huang W, Li D, Zhu Y, Tong Y, Zhang Y (2014) Porous $Pr(OH)_3$ nanowires as novel high-performance adsorbents for phosphate removal. Chem Eng J 252:202–209

[37] Kuroki V, Bosco GE, Fadini PS, Mozeto AA, Cestari AR, Carvalho WA (2014) Use of a La(III)-modified bentonite for effective phosphate removal from aqueous media. J Hazard Mater 274:124–131

[38] Dm B (2013) Batch sorption experiments: langmuir and Freundlich isotherm studies for the adsorption of textile metal ions onto teff straw (Eragrostis tef) agricultural waste. J Thermodyn 2013:1–6

[39] Al-Degs Y, Khraisheh MAM, Allen SJ, Ahmad MN (2000) Effect of carbon surface chemistry on the removal of reactive dyes from textile effluent. Water Res 34(3):927–935

[40] Li G, Gao S, Zhang G, Zhang X (2014) Enhanced adsorption of phosphate from aqueous solution by nanostructured iron(III)–copper(II) binary oxides. Chem Eng J 235:124–131

[41] Li H, Ru J, Yin W, Liu X, Wang J, Zhang W (2009) Removal of phosphate from polluted water by lanthanum doped vesuvianite. J Hazard Mater 168(1):326–330

[42] Olgun A, Atar N, Wang S (2013) Batch and column studies of phosphate and nitrate adsorption on waste solids containing boron impurity. Chem Eng J 222:108–119

[43] Weber WJMJC (1963) Kinetics of adsorption on carbon from solution. J Sanit Eng Div 89(2):31–60

[44] Jung K-W, Jeong T-U, Kang H-J, Ahn K-H (2016) Characteristics of biochar derived from marine macroalgae and fabrication of granular biochar by entrapment in calcium-alginate beads for phosphate removal from aqueous solution. Bioresour Technol 211:108–116

[45] Hui B, Zhang Y, Ye L (2014) Preparation of PVA hydrogel beads and adsorption mechanism for advanced phosphate removal. Chem Eng J 235:207–214

[46] Gu W, Xie Q, Qi C, Zhao L, Wu D (2016) Phosphate removal using zinc ferrite synthesized through a facile solvothermal technique. Powder Technol 301:723–729

[47] Zheng Y-M, Yu L, Wu D, Paul Chen J (2012) Removal of arsenite from aqueous solution by a zirconia nanoparticle. Chem Eng J 188:15–22

[48] Huang W-Y, Li D, Liu Z-Q, Tao Q, Zhu Y, Yang J, Zhang Y-M (2014) Kinetics, isotherm, thermodynamic, and adsorption mechanism studies of $La(OH)_3$-modified exfoliated vermiculites as highly efficient phosphate adsorbents. Chem Eng J 236:191–201

[49] Pu H, Liu Q, Liu G (2004) Methanol permeation and proton conductivity of acid-doped poly(N-ethylbenzimidazole) and poly(N-methylbenzimidazole). J Membr Sci 241(2):169–175

[50] Liu J, Zhou Q, Chen J, Zhang L, Chang N (2013) Phosphate adsorption on hydroxyl–iron–lanthanum doped activated carbon fiber. Chem Eng J 215:859–867

[51] Puziy AM, Poddubnaya OI, Ziatdinov AM (2006) On the chemical structure of phosphorus compounds in phosphoric acid-activated carbon. Appl Surf Sci 252(23):8036–8038

[52] Zhang G-S, Qu J-H, Liu H-J, Liu R-P, Li G-T (2007) Removal mechanism of As(III) by a novel Fe–Mn binary oxide adsorbent: oxidation and sorption. Environ Sci Technol 41(13):4613–4619

[53] Shin EW, Karthikeyan KG, Tshabalala MA (2005) Orthophosphate sorption onto lanthanum-treated lignocellulosic sorbents. Environ Sci Technol 39(16):6273–6279

[54] Chen N, Feng C, Zhang Z, Liu R, Gao Y, Li M, Sugiura N (2012) Preparation and characterization of lanthanum(III) loaded granular ceramic for phosphorus adsorption from aqueous solution. J Taiwan Inst Chem Eng 43(5):783–789

[55] Ning P, Bart H-J, Li B, Lu X, Zhang Y (2008) Phosphate removal from wastewater by model-La(III) zeolite adsorbents. J Environ Sci 20(6):670–674

[56] Tian S, Jiang P, Ning P, Su Y (2009) Enhanced adsorption removal of phosphate from water by mixed lanthanum/aluminum pillared montmorillonite. Chem Eng J 151(1–3):141–148

[57] Chen M, Huo C, Li Y, Wang J (2016) Selective adsorption and efficient removal of phosphate from aqueous medium with graphene-lanthanum composite. ACS Sustain Chem Eng 4(3):1296–1302